Atmos. Chem. Phys., 14, 9137–9153, 2014
www.atmos-chem-phys.net/14/9137/2014/
doi:10.5194/acp-14-9137-2014

Atmospheric Chemistry and Physics
Open Access

Ozone vegetation damage effects on gross primary productivity in the United States

X. Yue and N. Unger

School of Forestry and Environmental Studies, Yale University, 195 Prospect Street, New Haven, CT 06511, USA

Correspondence to: X. Yue (xu.yue@yale.edu)

Received: 14 November 2013 – Published in Atmos. Chem. Phys. Discuss.: 2 December 2013
Revised: 14 July 2014 – Accepted: 4 August 2014 – Published: 5 September 2014

Abstract. We apply an off-line process-based vegetation model (the Yale Interactive Terrestrial Biosphere model) to assess the impacts of ozone (O_3) vegetation damage on gross primary productivity (GPP) in the United States during the past decade (1998–2007). The model's GPP simulation is evaluated at 40 sites of the North American Carbon Program (NACP) synthesis. The ecosystem-scale model version reproduces interannual variability and seasonality of GPP at most sites, especially in croplands. Inclusion of the O_3 damage impact decreases biases of simulated GPP at most of the NACP sites. The simulation with the O_3 damage effect reproduces 64 % of the observed variance in summer GPP and 42 % on the annual average. Based on a regional gridded simulation over the US, summertime average O_3-free GPP is 6.1 g C m^{-2} day^{-1} (9.5 g C m^{-2} day^{-1} in the east of 95° W and 3.9 g C m^{-2} day^{-1} in the west). O_3 damage decreases GPP by 4–8 % on average in the eastern US and leads to significant decreases of 11–17 % in east coast hot spots. Sensitivity simulations show that a 25 % decrease in surface O_3 concentration halves the average GPP damage to only 2–4 %, suggesting the substantial co-benefits to ecosystem health that may be achieved via O_3 air pollution control.

1 Introduction

The effects of tropospheric ozone (O_3) damage on US forests have been studied for half a century (Karnosky et al., 2007), but the impacts of O_3 on the North American carbon balance are still relatively poorly understood (Felzer et al., 2004; Huntingford et al., 2011). O_3 is a secondary pollutant produced in the troposphere during the photochemical oxidation of carbon monoxide, methane, and volatile organic compounds (VOCs) by the major tropospheric oxidant, the hydroxyl radical, in the presence of sunlight and nitrogen oxides. Fossil-fuel, biofuel and biomass burning since the industrial and agricultural revolutions have greatly increased the emissions of O_3 precursors and led to an approximate doubling of O_3 levels over the US since the preindustrial. Deposition through stomatal uptake is an important sink for O_3 but damages photosynthesis, reduces plant growth and biomass accumulation, limits crop yields, and affects stomatal control over plant transpiration of water vapor between the leaf surface and atmosphere (Ainsworth et al., 2012; Hollaway et al., 2012).

Understanding the O_3 pollution influence on the North American forest sink is crucial to any effort to mitigate climate change by stabilizing atmospheric carbon dioxide (CO_2) concentrations. Currently, North America is acting as a net source of CO_2 to the atmosphere (King et al., 2012), mainly due to fossil-fuel combustion in the US and the deforestation in Mexico. Sequestration of atmospheric CO_2 by forest ecosystems is a major control on atmospheric CO_2 abundance and its growth rate (Pan et al., 2011). Terrestrial ecosystems of North America absorb the equivalent of about 35 % of North America's fossil fuel based CO_2 emissions, representing a source-to-sink ratio of nearly 3 : 1. Forest regrowth in the US is responsible for 30–70 % of this North American CO_2 sink, which varies significantly from year to year (Pacala et al., 2001; Goodale et al., 2002; Pan et al., 2011; King et al., 2012). However, O_3 damage may in part dampen the level of carbon sequestration by North American ecosystems (Felzer et al., 2004, 2005).

Experimental studies that examine O_3 impacts on plant productivity are typically performed for individual vegetation types, on the scale of sites, and within a limited time

period (e.g., Wittig et al., 2007; Feng et al., 2008; Lombardozzi et al., 2013). For example, based on measurements reported from over 100 studies, Wittig et al. (2007) estimated that chronic O_3 exposure depressed photosynthesis by 11 % and stomatal conductance by 13 % for several tree species at the ambient O_3 level of ∼ 45 ppbv relative to that in O_3-free air. The O_3 damage effect is strongest for crops. With data sets from ∼ 50 peer-reviewed studies, Feng et al. (2008) estimated that elevated O_3 levels significantly decrease wheat photosynthetic rates by 20 % and stomatal conductance by 22 %. Emerging research has found that the O_3 vegetation damage effects may result in a loss of plant stomatal control, and a consequent decoupling of the stomatal response from photosynthesis inhibition (Lombardozzi et al., 2012a, b, 2013).

Previous work has found that in the US region during 1989–1993, O_3 pollution reduced net primary productivity (NPP) by 3–7 % overall, and up to 13 % in hot spots including the southeast and in the Midwest agricultural lands (Felzer et al., 2004, 2005). The indirect CO_2 radiative forcing due to the vegetation damage effects of anthropogenic O_3 increases since the industrial revolution may be as large as $+0.4\,\mathrm{W\,m^{-2}}$ (Sitch et al., 2007), which is 25 % of the magnitude of the direct CO_2 radiative forcing over the same period, and of similar magnitude to the direct O_3 radiative forcing. Through this perturbation of the carbon cycle, O_3 pollution affects the climate system on considerably longer timescales than its own atmospheric lifetime (Unger and Pan, 2012). Over the past decade since this previous assessment surface O_3 levels in most of the US have decreased (Lefohn et al., 2010) due to domestic emission reductions following the implementation of air quality control legislation (Bloomer et al., 2010). However, increasing O_3 concentration is observed over western US (Jaffe and Ray, 2007). Such a trend may in part be related to the inter-continental flow from Asia (Cooper et al., 2010) and the global increase in methane (Rigby et al., 2008).

The major goal of this study is to assess O_3 damage effects on gross primary productivity (GPP) in the US for the recent decade 1998–2007 using a data-constrained vegetation model. In this work, we describe the implementation of a semi-mechanistic O_3 damage function (Sitch et al., 2007) into the Yale Interactive Terrestrial Biosphere model (YIBs) that includes enzyme-kinetic biophysics (Unger et al., 2013). In the first stage of the study, we utilize eddy-derived GPP flux measurements at 40 sites across the US and Canada that have been collated for the North American Carbon Program (NACP) site-level interim synthesis (Huntzinger et al., 2012; Schaefer et al., 2012; Barr et al., 2013; Ricciuto et al., 2013) to evaluate an off-line version of the vegetation model's site level GPP simulation and to assess the impact of surface O_3 damage at those sites. In the second stage of the study, the impacts of O_3 damage on GPP throughout the entire US are quantified using a regional configuration of the vegetation model.

2 Methodology and data

2.1 Vegetation biophysics

Here, we apply an off-line version of the YIBs model that previously was implemented into the NASA Goddard Institute for Space Studies global chemistry–climate model (Unger et al., 2013). The off-line model can be run at the site-level or in regional mode for a designated region. The vegetation biophysics module computes the photosynthetic uptake of CO_2 coupled with the transpiration of water vapor at the 1 h physical integration time step of the off-line model. The vegetation biophysics calculates C3 and C4 photosynthesis using the well-established Michealis–Menten enzyme-kinetics leaf model of photosynthesis (Farquhar et al., 1980; von Caemmerer and Farquhar, 1981) and the stomatal conductance model of Ball and Berry (Collatz et al., 1991). The coupled photosynthesis/stomatal conductance leaf model has been widely used to project terrestrial biosphere responses to global change. The model is briefly summarized here for transparency and completeness. The leaf model assumes that the rate of net CO_2 assimilation (A_{net}) in the leaves of C3 and C4 plants is limited by one of three processes: (i) the capacity of the ribulose 1,5-bisphosphate (RuBP) carboxylase-oxygenase enzyme (Rubisco) to consume RuBP (J_{c}); (ii) the capacity of the Calvin cycle and the thylakoid reactions to regenerate RuBP supported by electron transport (J_{e}); (iii) the capacity of starch and sucrose synthesis to consume triose phosphates and regenerate inorganic phosphate for photophosphorylation in C3 and phosphoenolpyruvate (PEP) limitation in C4 (J_{s}). J_{c}, J_{e}, and J_{s} are described as functions of the maximum carboxylation capacity (V_{cmax}) at the optimal temperature, 25 °C, and the internal leaf CO_2 concentration (C_{i}). The gross rate of carbon assimilation from photosynthesis (A) is given by the following:

$$A = \min(J_{\mathrm{c}}, J_{\mathrm{e}}, J_{\mathrm{s}}) \tag{1}$$

Net carbon assimilation is given by the following:

$$A_{\mathrm{net}} = A - R_{\mathrm{d}} \tag{2}$$

where R_{d} is the rate of dark respiration:

$$R_{\mathrm{d}} = 0.015 \cdot V_{\mathrm{c\,max}} \tag{3}$$

Leaf stomata control the uptake of CO_2 vs. the loss of H_2O. At equilibrium, the stomatal conductance of water vapor through the leaf cuticle (g_{s} in mol $[H_2O]\,\mathrm{m^{-2}\,s^{-1}}$) depends on the net rate of carbon assimilation:

$$g_{\mathrm{s}} = m\frac{A_{\mathrm{net}} \cdot \mathrm{RH}}{c_{\mathrm{s}}} + b = \frac{1}{r_{\mathrm{s}}} \tag{4}$$

where m and b are the slope and intercept derived from empirical fitting to the Ball and Berry stomatal conductance equations, RH is relative humidity, c_{s} is the CO_2 concentration at the leaf surface, and r_{s} is the stomatal resistance

to water vapor. Appropriate photosynthesis parameters for the local vegetation type are taken from (Friend and Kiang, 2005) and the Community Land Model (Oleson et al., 2010) with updates from Bonan et al. (2011) (Table 1). In both the site-level and regional models, we apply these model PFT-specific photosynthesis parameters and do not tune or calibrate to the local vegetation properties. The model calculates evapotranspiration as a function of the stomatal conductance. However, we do not consider the feedback of the changes in evapotranspiration to the boundary-layer meteorology because we use prescribed meteorological variables from reanalysis in the simulations.

The canopy radiative transfer scheme assumes a closed canopy and layers the canopy for light stratification using an adaptive number of layers (typically 2–16) (Friend and Kiang, 2005). Each canopy layer distinguishes sunlit and shaded regions for which the direct and diffuse photosynthetically active radiation (PAR) is computed (Spitters et al., 1986). The coupled photosynthesis and stomatal conductance equations are solved analytically using a cubic function of A_{net}. C_{i} is calculated explicitly at the leaf level. Scaling of the leaf to canopy level is through stratification of canopy light levels and leaf area profiles. The photosynthetic uptake of CO_2 is accumulated into a carbon reserve pool, from which other processes may allocate uses.

2.1.1 O_3 damage effect on photosynthesis

O_3 oxidizes cellular membranes and photosynthetic tissues when it enters leaves through stomata, leading to reductions in photosynthesis and GPP. O_3 damage inhibits stomatal conductance, which is closely related to the photosynthetic rate, resulting in a reduction in transpiration. A semi-mechanistic parameterization is employed to estimate the O_3 damage effects to both photosynthesis and stomatal conductance (Sitch et al., 2007). The exposure to O_3 leads to reductions in photosynthesis:

$$A' = F \cdot A_{\text{net}}, \tag{5}$$

where F is the reduction fraction calculated as

$$F = 1 - a \cdot U_{>\text{O3T}}, \tag{6}$$

where a is the O_3 sensitivity coefficient derived from observations. Two cases are examined: high and low O_3 sensitivity following Sitch et al. (2007). $U_{>\text{O3T}}$ is the instantaneous leaf uptake of O_3 flux above a plant function type (PFT)-specific threshold of O3T (Table 1),

$$U_{>\text{O3T}} = \max\left[\left(F_{\text{O}_3} - \text{O3T}\right), 0\right]. \tag{7}$$

Here F_{O_3} is the O_3 flux entering the leaf through the stomata,

$$F_{\text{O}_3} = \frac{[\text{O}_3]}{r_{\text{b}} + \kappa \cdot r'_{\text{s}}}, \tag{8}$$

where $[O_3]$ is the O_3 concentration at the top of the canopy, and r_{b} is the boundary layer resistance. The stomatal resistance to O_3 is calculated based on stomatal resistance to water r_{s} with a ratio constant $\kappa = 1.67$. From Eq. (4), the decrease in A_{net} reduces the stomatal conductance g_{s} proportionally,

$$r'_{\text{s}} = \frac{1}{g'_{\text{s}}} = \frac{1}{F \cdot g_{\text{s}}}. \tag{9}$$

The r'_{s} and g'_{s} are the O_3-damaged stomatal resistance and conductance, respectively. When the plant is exposed to $[O_3]$ (Eq. 8), the excess O_3 flux entering leaves (Eq. 7) causes $F < 1$ (Eq. 6), decreasing A_{net} (Eq. 5) while increasing the stomatal resistance (Eq. 9). The latter will act to reduce the O_3 uptake flux (Eq. 8) to protect the plant. Thus, the scheme considers associated changes in both photosynthetic rate and stomatal conductance. When photosynthesis is inhibited by O_3, the stomatal conductance decreases accordingly to resist more air passing through the stomata, resulting in a decline of the oxidant fluxes inside leaves, as described through Eqs. (5)–(9). Consequently, this coupled scheme represents the equilibrium state between the CO_2 demand for vegetation growth and the protection against O_3 damage by plant. The parameters for the scheme, including the O_3 damage threshold and sensitivity coefficients, were originally derived based on the calibration of the MOSES vegetation model. Since the MOSES model employs the (almost) identical Farquhar-Ball-Berry photosynthesis/stomatal conductance scheme as in the YIBs model, it is appropriate to adopt the same parameters as those derived in Sitch et al. (2007) (Table 1). Evaluation of the YIBs simulated O_3-induced GPP response with available field and laboratory measurements across a range of PFTs in Sect. 3.4 indicates that our assumption is reasonable.

2.1.2 Vegetation structure

The YIBs vegetation model simulates eight PFTs, using either C3 or C4 photosynthesis (Table 1). We apply two different sets of land cover and leaf area index (LAI) in the simulations. The first set is the PFT-specific vegetation cover fraction and LAI retrieved by the Moderate Resolution Imaging Spectroradiometer (MODIS, Knyazikhin et al., 1998). The value on a specific day is linearly interpolated from the monthly means of the nearest two months based on the distance of this day to the middle dates of those two months. The second set uses LAI from the Global Modeling and Assimilation Office (GMAO) Modern Era-Retrospective Analysis (MERRA) data set. The MERRA LAI is assimilated based on radiance data retrieved by over 20 satellites (Rienecker et al., 2011) and is available on a daily scale from 1980 onwards. Since the MERRA LAI data set does not provide PFT-specific information, the actual site-level PFT is assumed for the site level simulations. For the regional simulations, the land cover is prescribed to the gridded International

Table 1. Parameters for vegetation model and O_3 damage scheme.

PFT[a]	TDA	GRAC3	GRAC4	SHR	DBF	ENF	TRF	CRO	
Carboxylation	C3	C3	C4	C3	C3	C3	C3	C3[b]	C4[b]
$V_{max\,25}$ (μmol m^{-2} s^{-1})	33	43	24	25	30	43	75	40	40
m	9	11	5	9	9	9	9	11	5
b (mmol m^{-2} s^{-1})	2	8	2	2	2	2	2	8	2
O3T (nmol m^{-2} s^{-1})	1.6	5	5	1.6	1.6	1.6	1.6	5	5
a (high) (mmol^{-1} m^{-2})	0.1	1.4	0.735	0.1	0.15	0.075	0.15	1.4	0.735
a (low) (mmol^{-1} m^{-2})	0.03	0.25	0.13	0.03	0.04	0.02	0.04	0.25	0.13

[a] Plant function types (PFTs) are tundra (TDA), C3 grassland (GRAC3), C4 savanna/grassland (GRAC4), shrubland (SHR), deciduous broadleaf forest (DBF), evergreen needleleaf forest (ENF), tropical rainforest (TRF), and cropland (CRO).
[b] For site-level simulations, we consider CRO to be a C4 plant. For regional simulation, we consider half CRO as C3 plants (soybean) and the rest C4 plant (corn).

Satellite Land-Surface Climatology Project (ISLSCP, Hall et al., 2006).

2.1.3 Meteorological forcing

For the site-level simulations, we use hourly in situ measurements of surface meteorological variables, including surface air temperature, specific humidity, wind speed, surface pressure, and CO_2 concentrations. There are some missing values in the measurements due to occasional instrument failure. We gap-fill the site-based observations with that from the MERRA-land data (Reichle et al., 2011), which is interpolated to each site based on the site location.

For the regional simulations, the off-line YIBs model uses hourly MERRA-land data climatic variables including the following: surface air temperature, specific humidity, wind speed, surface pressure, precipitation, direct PAR, and diffuse PAR, and soil temperature and soil moisture at six soil depths. The original data resolution of $0.5° \times 0.667°$ by latitude and longitude is degraded to $1° \times 1.333°$ due to current disk space limitation.

2.1.4 Surface [O_3]

Hourly and daily maximum 8 h average surface [O_3] representative of the present day climate ($\sim$2005) are taken from previous simulations using NASA Model-E2 (Shindell et al., 2013). The global model has $2° \times 2.5°$ latitude by longitude horizontal resolution with 40-vertical layers extending to 0.1 hPa. The gas-phase chemistry and aerosol modules are fully integrated, so that these components interact with each other and with the physics of the climate model (Bell et al., 2005; Shindell et al., 2006, 2013; Unger, 2011). The model surface O_3 is validated using measurements from 73 Clean Air Status and Trends Network (CASTNET) sites operated by the United States Environmental Protection Agency (EPA) (http://epa.gov/castnet/javaweb/ozone.html) and $\sim$1200 monitor sites managed by the EPA AIRDATA (http://www.epa.gov/airdata/). These sites are operated on the county level scale. The CASTNET provides hourly [O_3] at rural sites from 1996–2005. The AIRDATA network provides daily maximum 8 h average (MDA8) [O_3], covering both urban and rural regions. We use AIRDATA data for the year 2005.

2.2 Simulations

2.2.1 Site-level runs

We configure a site-level version of the YIBs model for the 40 eddy covariance flux tower sites described in detail in the NACP synthesis (Fig. S1 in the Supplement and Appendix Table A1, Schaefer et al., 2012). Meteorological measurements are available for a wide range of time periods across the different sites ranging from the minimum of 1 year at Fermi Lab (US-IB1) and the maximum of 15 years at Harvard Forest (US-HA1). These sites cover a range of different vegetation types including the following: evergreen needleleaf forest (ENF), deciduous broadleaf forest (DBF), grasslands, croplands, closed shrublands, mixed forests, permanent wetlands, and woody savannas. Table S1 in the Supplement summarizes how the NACP vegetation types are mapped onto the eight model PFTs. For the site-level simulations, we assume C4 photosynthetic pathway for all cropland sites, which are mainly corn (Schaefer et al., 2012). The local site LAI values are not available. As a result, we use the MERRA or MODIS LAI for the simulations.

For each site, a group of six sensitivity simulations are performed (Table 2). We conduct the first four runs using different combinations of meteorological and vegetation forcings,

to assess the sensitivity of the results to local vs. reanalysis meteorological forcing and LAI (Table 2). Two, METmerra_LAImodis and METmerra_LAImerra, use hourly meteorology from MERRA-land reanalyses alone. The other two, METsite_LAImodis and METsite_LAImerra, use site-based meteorology with gap-filled MERRA reanalysis. Simulations use two data sets of LAI: (1) METmerra_LAImerra and METsite_LAImerra use LAI from the MERRA-land reanalyses, which provide non PFT-specific LAI that we assign to the local PFT type at each site (Table A1), while (2) METmerra_LAImodis and METsite_LAImodis use PFT-specific LAI retrieved by the MODIS. Later analyses show that METsite_LAImerra has the lowest biases relative to other O_3-free simulations. We perform two additional site-level simulations, which use the same forcings as that for METsite_LAImerra but with the impact of O_3 uptake on photosynthesis. These two experiments, METsite_LAImerra_HO3 and METsite_LAImerra_LO3, use either high or low O_3 sensitivity as defined by the coefficient a in Table 1.

To quantify the performance of the vegetation model, we estimate the χ^2 for each site following the method described in Schaefer et al. (2012),

$$\chi^2 = \frac{1}{n}\sum_{i=1}^{n}\left(\frac{r_i}{\varepsilon_i}\right)^2, \quad (10)$$

where

$$r_i = (\mathrm{GPP_{si}} - \mathrm{GPP_{oi}}). \quad (11)$$

is the difference between the pair of simulated and observed GPPs. ε_i are the observational uncertainties resulting from turbulence, gap-filling, flux partitioning, and u^* threshold determination (Barr et al., 2013). n is the length of observations (e.g., the number of days for the daily variables). The lower the χ^2, the smaller the model biases. If $\chi^2 < 1$, the simulation bias is on average smaller than the measurement uncertainty, indicating a good performance of the model. Here, we define a reasonable performance of $\chi^2 < 4$, when the residual is less than twice the measurement uncertainty. We also calculate the root mean square error (RMSE) as follows:

$$\mathrm{RMSE} = \sqrt{\frac{1}{n}\sum_{i=1}^{n}(\mathrm{GPP_{si}} - \mathrm{GPP_{oi}})^2}. \quad (12)$$

We validate the simulated O_3 damage effect with measurements from literature. Field and laboratory experiments may have different $[O_3]$ compared to the ambient level we used complicating the validation. As a result, we perform 14 additional sensitivity simulations for each of NACP sites. All tests use meteorological and vegetation forcings the same as METsite_LAImerra (Table 2), except for the different $[O_3]$ and O_3 sensitivity. These experiments are divided into two groups, seven in each, using either low or high O_3 sensitivity. In each group, simulations are performed with constant $[O_3]$ at 20, 40, 60, 80, 100, 120, 140 ppbv, respectively. We do not include diurnal and seasonal variations of $[O_3]$ in these sensitivity simulations as that in METsite_LAImerra for two reasons. First, field measurements for the O_3 vegetation damage are usually performed with fixed $[O_3]$ during the growth season (e.g., Ishii et al., 2004; Zhang et al., 2012). Second, the diurnal cycles and seasonality of $[O_3]$ are very different for different sites (Bloomer et al., 2010), making it difficult to apply a uniform temporal cycle for all the NACP sites. The reductions in GPP at these simulations are compared with results from field measurements at the corresponding $[O_3]$ level.

2.2.2 Regional run over US

A gridded version of the YIBs model at $1^\circ \times 1.333^\circ$ latitude by longitude horizontal resolution for the US region is driven with MERRA meteorological forcings for the period 1998–2007. In the regional model, vegetation cover types are from the ISLSCP and LAI is form the MERRA-land reanalysis. We assign the MERRA LAI to the corresponding PFT types defined by ISLSCP (Fig. S2 in the Supplement). The 18 ISLSCP land types are converted to 8 PFTs used in the model (Table S1 in the Supplement). Some of the ISLSCP land types, such as the deciduous needleleaf forest, are not represented in the YIBs model. However, the coverage of these types is very small in the US (Fig. S2 in the Supplement) and will not influence the regional simulation after the conversion to the model types. For the regional simulation, we assume that the total crop area in each crop grid cell is split 50 % C3 and 50 % C4 to account for the dominance of both soybean (C3) and corn (C4) crops in the central and northern US agricultural regime. We perform two simulation cases with high and low O_3 damage sensitivity. Finally, to understand how the O_3 vegetation damage effect may respond to possible future changes in $[O_3]$, we perform four additional sensitivity experiments with ± 25 % changes in $[O_3]$ for each O_3 sensitivity case.

3 Results and discussion

3.1 Evaluation of O_3-free GPP at NACP sites

We first compare the monthly mean LAI from MERRA and MODIS at each NACP site (Fig. S3 in the Supplement). For each site, the MERRA LAI is averaged for the period when GPP measurements are available. The two data sets show similar annual cycles at several sites but are inconsistent for 7 out of 20 ENF sites (CA-Ca1, CA-Ca2, CA-Ca3, CA-NS1, US-Me2, US-Me3, and US-Me5) and 2 out of 5 shrubland sites (US-SO2 and US-Ton). In addition, for grasslands and croplands, the data sets exhibit different seasonality. It must be emphasized that the MERRA and MODIS LAI represent the average state in the retrieval product grid cells and as such

Table 2. Description of the site-level simulations.

		Meteorology		Vegetation (LAI)		
ID	Simulations[a]	Site	MERRA	MODIS	MERRA	Incl. O_3^c
1	METmerra_LAImodis		Yes	Yes		
2	METsite_LAImodis[b]	Yes	Yes	Yes		
3	METmerra_LAImerra		Yes		Yes	
4	METsite_LAImerra[b]	Yes	Yes		Yes	
5	METsite_LAImerra_LO3[b]	Yes	Yes		Yes	Low[d]
6	METsite_LAImerra_HO3[b]	Yes	Yes		Yes	High [d]

[a] The name of each simulation is composed of at least two words. The prefix indicates the source of meteorological forcings. The suffix or the second word indicates the sources of vegetation forcings.
[b] For simulations with prefix "SITE" use site-based meteorological forcings, which are gap-filled with MERRA-land reanalyses.
[c] Ambient $[O_3]$ is applied at each site.
[d] Low and high indicate the sensitivity of GPP to $[O_3]$ defined by the coefficient a in Table 1.

may not represent the local LAI for the actual PFT species at each site.

The long-term monthly mean O_3-free GPP from the simulation METsite_LAImerra is compared with observations at NACP sites (Figs. 1 and S4 in the Supplement). The simulations capture the magnitude and seasonality of GPP for most sites especially for deciduous broadleaf and cropland. The largest model overestimate (factor of 3–8) occurs at two ENF sites, CA-SJ1 and CA-SJ2 in North Central Canada (Fig. S4 in the Supplement). For the grassland sites, the model–observation correlation is low because the seasonality is not well captured, especially for US-ARM (in Great Plains) and US-Var (in California), where the modeled maximum GPP occurs in summer (July), 2–3 months later than in the measurements (April) (Fig. S4 in the Supplement). This incorrect model seasonality is a result of the MERRA LAI (compare Fig. S3 in the Supplement) that does not begin to increase rapidly until after May and is not consistent with the local LAI at the site. In reality, California grasslands exhibit rapid growth in spring then mature and die after April or May (Chiariello, 1989). The grasslands in the Great Plains may have up to six different phenological groups, including some species active in spring (e.g., in US-ARM) while some others peak in summer (e.g., in US-Shd) (Henebry, 2003). On the annual mean basis, the correlation coefficient between simulated GPP and observations at all 40 sites is 0.65. The correlation is higher (0.81) for summer (June–August, Fig. S5 in the Supplement). The annual GPP averaged over all 40 sites is 3.8 g C m^{-2} day^{-1}, 27 % higher than the observational average (3.0 g C m^{-2} day^{-1}).

Among the 40 NACP sites, 22 have reasonable performance with $\chi^2 < 4$ for the simulation METsite_LAImerra (Fig. 2a). For these sites, 12 are ENF with the best ($\chi^2 = 1.2$) at site US-Dk3 (Fig. S4 in the Supplement). The ENF sites usually have multiple years of measurements and provide good samples for testing the consistency between simulations and observations. Simulations at other four DBF, three cropland, and three shrubland sites have $\chi^2 < 4$. Compared

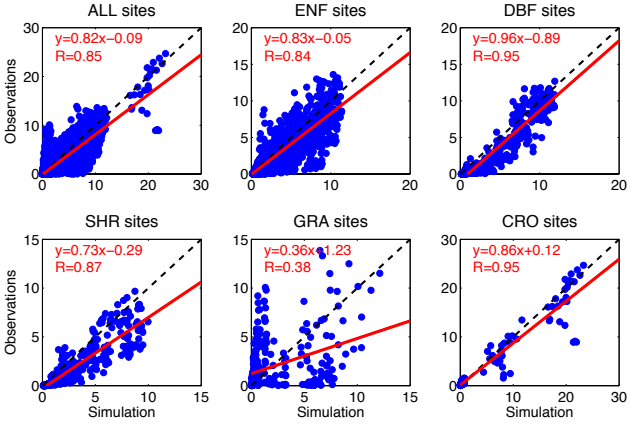

Figure 1. Comparison between monthly average GPP in the YIBs simulations and NACP observations grouped by PFT type (where in situ measurements are available). The red lines indicate linear regression between observations and simulation results. The regression fits and correlation coefficients are shown on each panel. The land types include evergreen needleleaf forest (ENF), deciduous broadleaf forest (DBF), shrublands (SHR), grasslands (GRA), and croplands (CRO). The model–observation comparison for each site is shown in Fig. S4 in the Supplement.

with the 24 land surface models in Schaefer et al. (2012), the YIBs model shows significant improvement at the crop PFT sites ($\chi^2 < 4.1$ vs. $\chi^2 > 6$). YIBs simulates GPP with $\chi^2 < 4$ at 22 sites in total compared to 16 sites for the ensemble simulations in Schaefer et al. (2012). YIBs GPP simulation is weaker ($\chi^2 > 4$) at 18 sites including eight ENF sites, two DBF, and two shrubland PFT sites. The common feature of the biases at these sites is the overestimation of peak GPP during summer (e.g., CA-SJ1, CA-SJ2, CA-Mer, Fig. S4 in the Supplement). It is possible that the model does not represent the full realism of the biophysical processes accurately. However, we assert that the most likely cause of the model overestimate is the uniform application of model

PFT-specific photosynthesis parameters that are not tuned to local site level vegetation parameters and, for instance, do not take into account plant species and age. Similar to the multi-model results in Schaefer et al. (2012), YIBs performance is weakest at the five grassland sites. In this case, the bias is mainly due to the delayed LAI seasonality in the MERRA satellite data set (Figs. S3 and S4 in the Supplement). In general, application of the remotely sensed LAI is a source of error because the gridded satellite data may not represent the local site changes in plant growth and phenology, especially for vegetation types with low biomass. The limitation of the satellite LAI spatial resolution implies that the model is unable to resolve GPP variability for sites in close proximity. For example, sites CA-SJ1, CA-SJ2, and CA-SJ3 are located close to each other. Simulations at these sites have similar magnitude in simulated GPP while observations show distinct variability between the sites.

We compare R^2, RMSE, and χ^2 for the different sensitivity experiments in order to ascertain which combination of meteorological and LAI forcings best reproduces the measured GPP over North America (Table 3 and Fig. 3). The sites CA-Let, CA-NS1, US-Var, CA-SJ1, and CA-SJ2 are excluded from the analysis because of excessive bias(Fig. S6a in the Supplement). The average R^2 increases while RMSE decreases when MERRA reanalyses are substituted with site-based meteorology, or the MERRA LAI is used instead of MODIS LAI (Table 3). The choice of LAI forcing has the most significant impact on YIBs simulation performance, consistent with previous work that showed the dominance of phenology over meteorology in controlling local terrestrial carbon exchange (Desai et al., 2008; Puma et al., 2013). Using MODIS LAI, YIBs has a total χ^2 of 9.2 that shows an average reduction of 4.7 (52 %) with MERRA LAI (Table 3 and Fig. 3). Applying the site meteorology relative to MERRA meteorological forcings offers smaller improvements. For example, the total χ^2 value decreases by 5 % in METsite_LAImodis compared with that in METmerra_LAImodis and 15 % in METsite_LAImerra relative to that in METmerra_LAImerra (Table 3).

3.2 Evaluation of modeled surface [O_3]

We validate summertime surface O_3 simulated by the NASA Model-E2 chemistry–climate model with observations from the CASTNET and AIRDATA (Fig. 4). High O_3 level appears in the eastern US due to anthropogenic emissions and in the mountainous western US due to high elevation. The model generally captures this spatial pattern with a correlation coefficient of 0.39 against observations over the selected 73 CASTNET sites (Fig. 4a–b). The simulation overestimates the O_3 level by $\sim$4 ppbv (12 %) in the east and $\sim$1 ppbv (3 %) in the west. The CASTNET sites are located in rural sites, which usually have lower [O_3] than that in urban areas, except for some megacities where the excessive NO_x emissions result in lower O_3 level (Gregg et al., 2003).

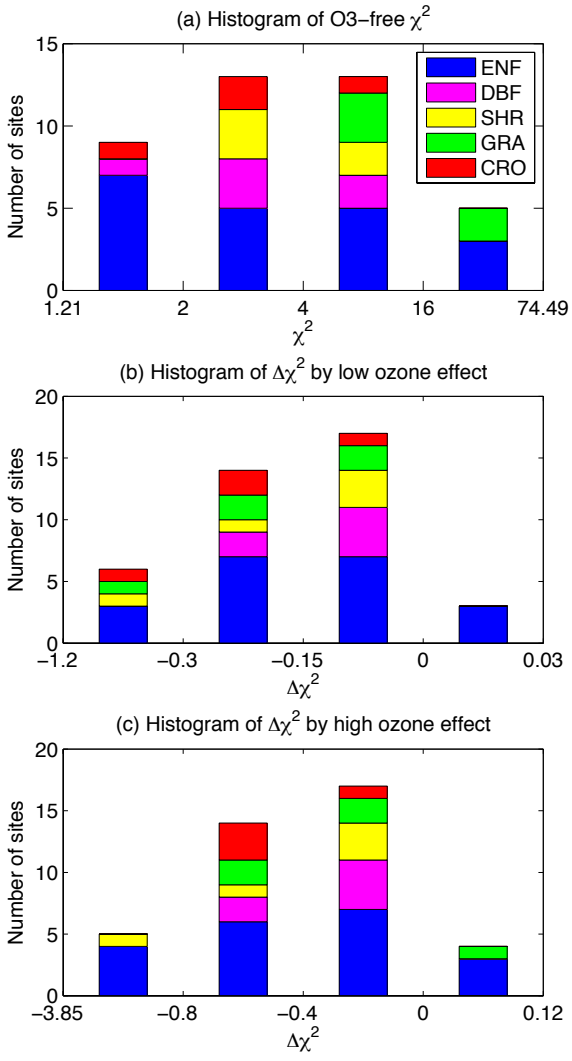

Figure 2. Histogram of **(a)** χ^2 for O_3-free GPP and changes in χ^2 after the inclusion of O_3 damage impact with **(b)** low and **(c)** high O_3 sensitivity. Each bar represents the number of sites where the χ^2 or $\Delta\chi^2$ of simulations fall between the specific thresholds as defined by the x axis intervals. The minimum and maximum of χ^2 or $\Delta\chi^2$ are indicated as the two ends of x axis in the plots. The land cover definitions are as follows: ENF, Evergreen Needleleaf Forest; DBF, Deciduous Broadleaf Forest; SHR, Shrubland; GRA, Grasslands; CRO, Croplands. Results for each site are detailed in Fig. S6 in the Supplement.

Therefore, we also compare the simulated MDA8 [O_3] with monitored at $\sim$1200 AIRDATA sites, which covers both urban and rural regions (Fig. 4c). In the eastern US, the model captures high [O_3] centers around Michigan, Indiana, and Ohio states and that along the northeast coast. In the west, the simulation reproduces high [O_3] over mountain regions and in California. On average, the simulated MDA8 [O_3] is lower by $\sim$0.5 ppbv (1 %) in the east and $\sim$3.5 ppbv (7 %)

Table 3. Statistics* for site-level simulations.

		R^2			RMSE			χ^2		
ID	Simulations	min	max	mean	min	max	mean	min	max	total
1	METmerra_LAImodis	0.14	0.85	0.63	1.2	6.4	3.0	1.4	37.6	9.4
2	METsite_LAImodis	0.16	0.85	0.67	1.1	5.8	2.9	1.1	39.6	8.9
3	METmerra_LAImerra	0	0.88	0.66	1.3	4.2	2.4	1.2	16.6	4.8
4	METsite_LAImerra	0	0.87	0.68	1.0	4.2	2.3	1.2	13.4	4.1
5	METsite_LAImerra_LO3	0	0.88	0.69	1.0	4.1	2.3	1.1	13.0	3.9
6	METsite_LAImerra_HO3	0	0.88	0.69	1.0	4.1	2.2	1.0	12.3	3.7

* Statistics include minimum and maximum values of R^2, RMSE, and χ^2 for 35 NCAP sites with $\chi^2 < 16$ (Fig. S6a in the Supplement). We also calculate the mean values of R^2 and RMSE for these sites. We calculate the total χ^2 (shown as red bars in Fig. 3) using all the available observations over all sites.

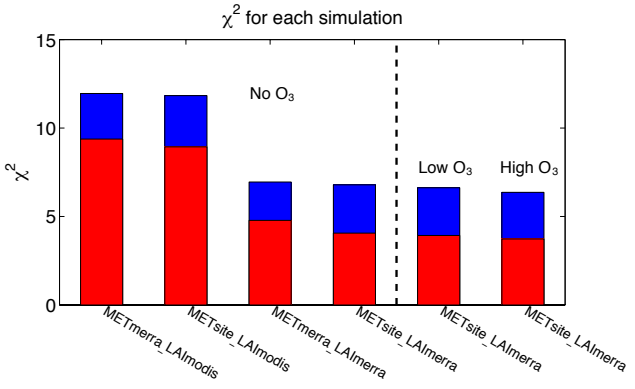

Figure 3. The calculated average χ^2 of GPP over NACP sites for six different simulations as listed in Table 2. The blue bars are results for all 40 NACP sites. The red bars are results excluding sites CA-Let, CA-NS1, US-Var, CA-SJ1, and CA-SJ2, where the simulated site-level χ^2 is larger than 16 as shown in Fig. S6a in the Supplement.

in the west. The correlation coefficient between simulations and observations is as high as 0.51 (Fig. 4d).

3.3 O_3 damage effects at NACP sites

We must apply the simulated O_3 to quantify the O_3 vegetation damage at the NACP sites because the sites do not monitor local [O_3]. The summer average [O_3] is 30–50 ppbv at 24 US sites (Fig. 5a). The O_3 damage effect is relatively stronger at sites with both high O_3-free GPP and ambient [O_3] (Fig. 5d). The most significant damages are predicted at US-MMS (DBF) and US-Dk3 (ENF) sites, where the GPP reductions are 5–14 % depending on the low or high O_3 sensitivity (Fig. 5d). At these two sites, the high stomatal conductance (4.0 and 3.4 mm s^{-1}, Fig. 5b) and ambient [O_3] (both 43 ppbv, Fig. 5a) result in the largest O_3 stomatal flux (both ~ 0.3 mmol m^{-2} d^{-1}, Fig. 5c) among the 24 sites. The lowest O_3 damage (1–2 % GPP reduction) appears in the three shrub sites, US-Ton, US-SO2, and US-Los, although mean [O_3] there is as high as 43 ppbv. The main reason for the limited O_3 damage is the low stomatal conductance (average 1.4 mm s^{-1}, Fig. 5b) related to the small O_3-free GPP (average 4.6 g C m^{-2} d^{-1}, Fig. 5d). Similarly, the O_3 damage for C3 grass is as low as 1–2 %, although the GPP of this plant is highly sensitive to O_3 (Table 1). For ENF and DBF sites, the average site-level O_3 damage effects are estimated to be 2–5 and 3–9 % respectively with differences between these ecosystem types predominantly driven by differences in sensitivity to O_3. The four C4 crop sites, US-Ne1, US-IB1, US-Ne2, and US-Ne3, exhibit the highest O_3-free GPP but show only moderate O_3 damage effects (GPP reductions of 4–6 %, Fig. 5d). This result is driven by low ambient [O_3] at the C4 crop sites (average 32 ppbv, Fig. 5a) in combination with the reduced C4 stomatal conductance (higher water use efficiency) relative to C3 plants (average 3.2 mm s^{-1}, Fig. 5b). Indeed, the C4 photosynthetic pathway has been observed to offer protection against O_3 damage (Heagle et al., 1989; Rudorff et al., 1996).

Inclusion of O_3 damage effect improves the site-level simulations (Fig. 2b–c). For 36 out of the 40 sites, the χ^2 of simulated GPP decreases when considering vegetation responses to O_3, and the improvement is better when higher O_3 sensitivity is applied. At these sites, for example, CA-TP4, US-Dk3, US-MMS, and US-PFa, the reduced GPP at peak seasons is closer to measurements (not shown), leading to smaller biases for simulations. On average, the χ^2 decreases by 3–8 % at these sites, depending on the O_3 sensitivity in the simulation (Table 3 and Fig. 3). Finally, the simulated annual GPP averaged over all NACP sites changes from 3.8 g C m^{-2} day^{-1} to 3.6 g C m^{-2} day^{-1} with the high O_3 sensitivity simulation case, closer to the observations of 3.0 g C m^{-2} day^{-1}. The bias-correction from O_3 damage is much smaller relative to the effect of phenology (Fig. 3). Moreover, the O_3-induced damage does not improve the GPP correlation between observations and simulations, which remains similar at ~ 0.8 (for 40 sites) with and without O_3 effects (Fig. S5 in the Supplement).

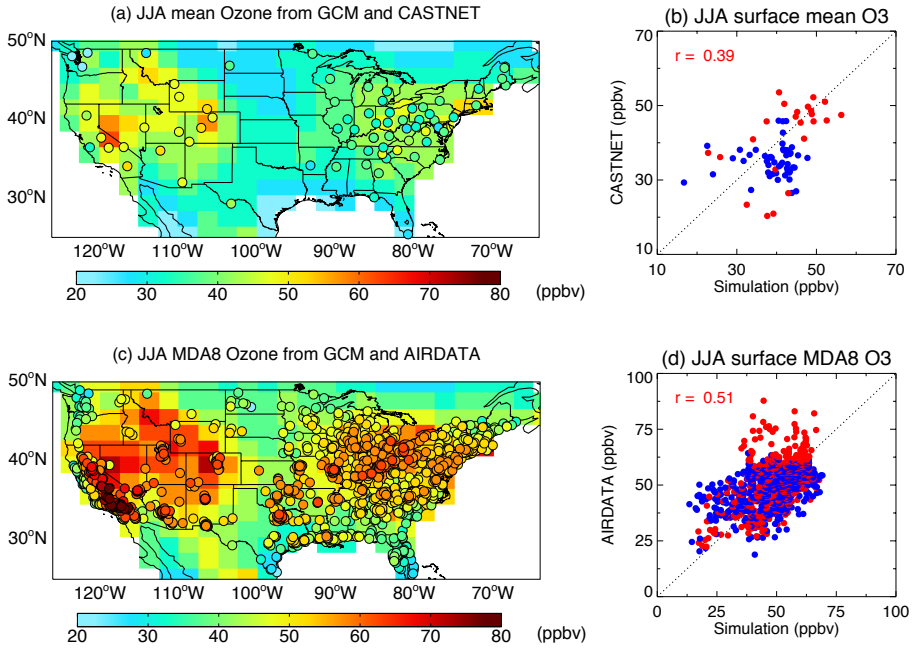

Figure 4. Validation of simulated June–July–August (JJA) summertime average surface **(a, b)** diurnal mean and **(c, d)** daily maximum 8 h average O_3 with in situ measurements from **(a, b)** the EPA Clean Air Status and Trends Network (CASTNET) and **(c, d)** the AIRDATA. For **(b)** and **(d)**, the blue points indicate sites east of 95° W and the red points indicate sites west of 95° W. The correlation coefficients are shown in **(b)** and **(d)**. Each point in **(b)** and **(d)** represents the mean value for JJA at one specific site. Results for the model and observations are separated out in Fig. S7 in the Supplement.

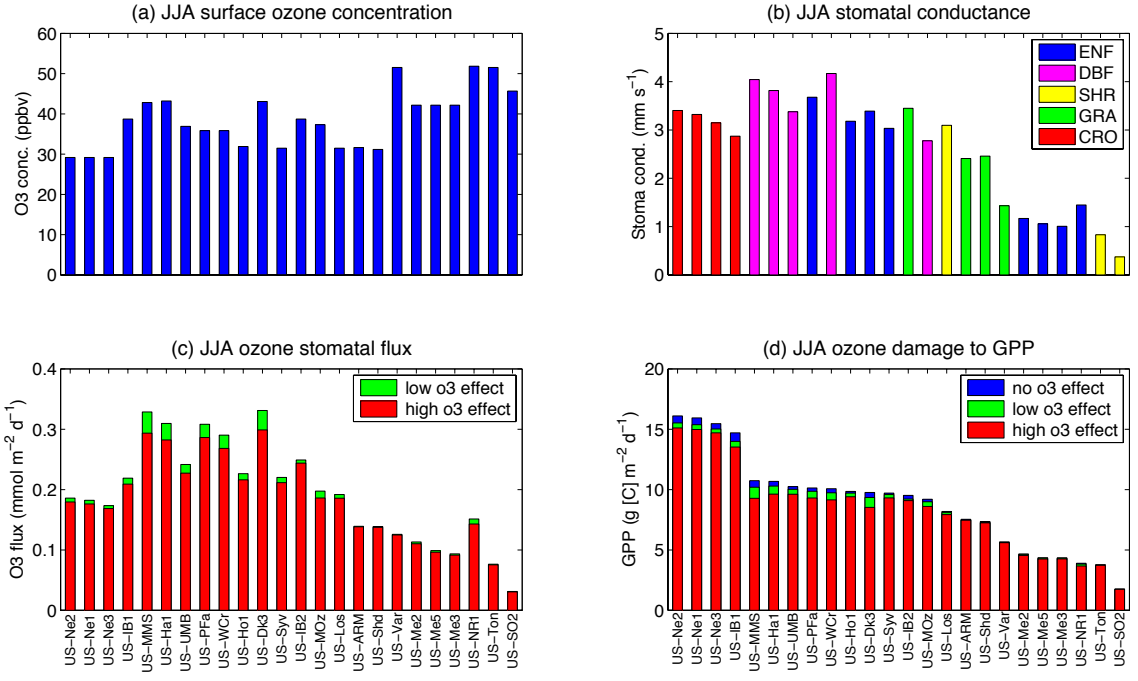

Figure 5. Simulated June–July–August (JJA) summertime average **(a)** surface [O_3], **(b)** stomatal conductance, **(c)** ozone stomatal flux, and **(d)** damages to GPP at different O_3 sensitivity for 24 US sites. The sites are sorted according to the simulated O_3-free GPP in **(d)**. For each site, the result represents the average over the period when the site GPP measurements are available during JJA. The land cover definitions are as follows: ENF, evergreen needleleaf forest; DBF, deciduous broadleaf forest; SHR, shrubland; GRA, grasslands; CRO, croplands.

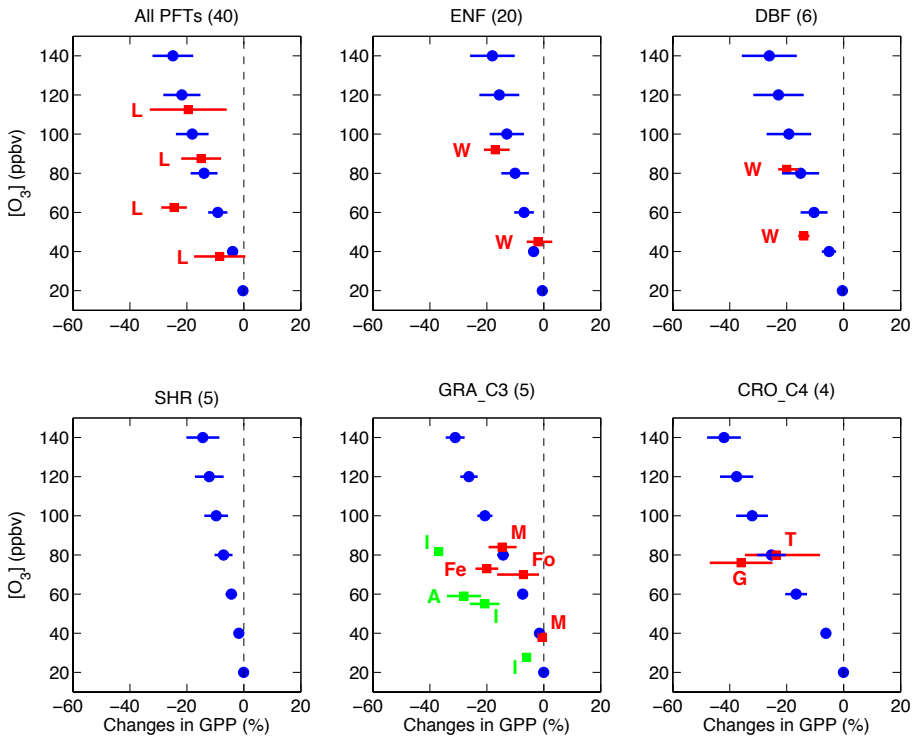

Figure 6. Percentage change in GPP (%) averaged across all sites and grouped by individual PFT type in the presence of different levels of $[O_3]$ as simulated by the YIBs vegetation model. Simulations are performed at 40 NACP sites with a prescribed fixed $[O_3]$ for either low or high O_3 sensitivity. Blue points indicate the average model reduction with the blue horizontal lines indicating the damage range across low to high O_3 sensitivity. The number of sites used to obtain the average reduction value is shown in the title bracket of each subplot. The solid squares with lines show the results (mean plus uncertainty) based on measurements reported in multiple studies. Measurements include the following: Lombardozzi et al. (2013) for all PFTs; Wittig et al. (2007) for evergreen needleleaf forest (ENF) and deciduous broadleaf forest (DBF); C4 grass or crop (CRO_C4) from Taylor et al. (2002) for *spartina alterniflora* and Grantz et al. (2012) for sugarcane hybrids; C3 grass or crop (GRA_C3) from Feng et al. (2008) for wheat, Foot et al. (1996) for *colluna vulgaris*, Mulchi et al. (1992) for soybean, and Ishii et al. (2004) and Ainsworth (2008) for rice. Values for rice are denoted in green and others in red. The author initials are indicated for the corresponding studies.

3.4 Evaluation of simulated O_3 vegetation damage against field and laboratory data

We compare the simulated O_3 damage effect with field and laboratory measurements from the published literature (Fig. 6). In total, 14 additional sensitivity experiments are performed with different levels of $[O_3]$ at each NACP site (see Sect. 2.2.1). GPP reductions increase accordingly with the increasing $[O_3]$ (Fig. 6). For a given $[O_3]$, the O_3 damage effect is strongest for C4 crops (despite the lower $g_s : A_{net}$ ratio) but weakest for shrubland. YIBs simulates reasonable O_3 damage to GPP for all model PFTs compared to the meta-analyses of Wittig et al. (2007) and Lombardozzi et al. (2013). Field studies in shrubland are limited. Zhang et al. (2012) investigated the responses of four shrub species to $[O_3] = 70$ ppbv and found large reductions in net photosynthesis of 50–60 %. The average O_3-free A_{net} of those shrub species was 8–16 g [C] m^{-2} s^{-1}, much higher than even the gross photosynthesis (A) of 6 g [C] m^{-2} s^{-1} at the shrub NACP sites, likely because the latter are located in dry and/or cold areas (Fig. S1 in the Supplement). The YIBs simulated O_3 vegetation damage effects for C4 plants are in good agreement with field measurements from Taylor et al. (2002) and Grantz et al. (2012). In the case of C3 grass and C3 crop, the model simulates consistent GPP reduction percentages with observations from Feng et al. (2008) for wheat, Foot et al. (1996) for *colluna vulgaris*, and Mulchi et al. (1992) for soybean. However, these O_3 damage results are all > 50 % less than for available measurements in rice crops (Ishii et al., 2004; Ainsworth et al., 2008), suggesting that rice may have much higher O_3 sensitivity than other C3 plants. In the US rice plantation area is much smaller than that of soybean and corn. Therefore, we adopt the O_3 sensitivity parameters for C3/C4 plants shown in Table 1 for the regional simulations.

3.5 O_3 vegetation damage effect on GPP in US region

High values of simulated summertime GPP (including O_3 damage effect) appear east of 95° W in the US (Fig. 7a),

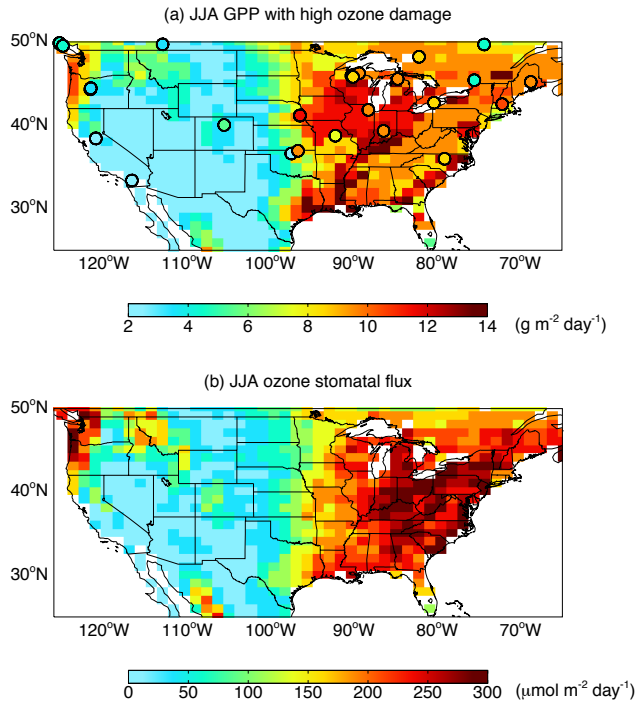

Figure 7. Simulated summertime **(a)** O_3-exposed GPP and **(b)** O_3 stomatal flux over the US. The simulated GPP is overlaid with in situ measurements from NACP. The simulations are performed with land cover from ISLSCP and meteorological forcings from MERRA reanalysis. Figure S8 in the Supplement separates results for model and measurements.

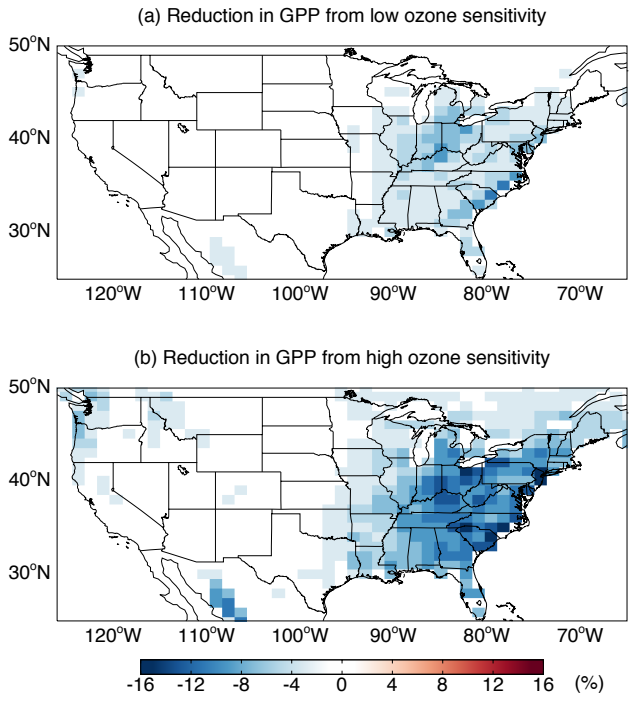

Figure 8. Simulated reduction fraction in summer GPP in the US due to **(a)** low and **(b)** high O_3 sensitivity for 1998–2007.

because the land surface there is covered by crops and forests. A high center of GPP ($> 10\,\mathrm{g\,C\,m^{-2}\,day^{-1}}$) appears over cropland in the north central US In the western US, the coverage of grass and shrub and the low water availability (low precipitation and soil moisture) over semi-arid regions lead to a low carbon-assimilation rate. The regional gridded simulated GPP reproduces the JJA growing season average NACP site-level fluxes with a correlation coefficient of 0.62 for 32 sites below 50° N (points in Fig. 7a). The correlation is lower than the 0.84 estimated for the site-level simulation METsite_LAImerra at the same sites and the same season. Since the meteorological forcings and LAI are similar, the difference in land cover, ISLSCP vs. site definitions (Figs. S1 and S2 in the Supplement), accounts for the discrepancy between regional and site-level simulations.

On average, the simulated summer GPP (including the high O_3 damage effect) is $9.5\,\mathrm{g\,C\,m^{-2}\,day^{-1}}$ in the eastern US (east of 95° W) and $3.9\,\mathrm{g\,C\,m^{-2}\,day^{-1}}$ in the western US (west of 95° W), giving a mean value of $6.1\,\mathrm{g\,C\,m^{-2}\,day^{-1}}$ for the US region. The total carbon uptake is estimated to be $4.43 \pm 0.18\,\mathrm{Pg\,C}$ during the summer growing season, accounting for 57–60 % of the annual average value of $7.59 \pm 0.25\,\mathrm{Pg\,C}$ over the 1998–2007 period. Our estimate of annual carbon uptake is consistent with previous published estimates. For example, Xiao et al. (2010) upscaled site-level GPP flux to continental scale with a regression tree approach based on both NACP fluxes and remote-sensing variables. They estimated that the total GPP in US ranges from 6.91 to 7.33 Pg C per year during 2000–2006. Using the same observations but with a process-based biogeochemical model, Chen et al. (2011) estimated a range of 7.02–7.78 Pg C per year for 2000–2005, which is even closer to our estimate.

We calculate both O_3 stomatal flux (Fig. 7b) and the resultant damage on GPP (Fig. 8) in the US region for the 1998–2007 period. High O_3 stomatal flux is predicted in the eastern US due to co-location of the high GPP (medium to high stomatal conductance) and the substantial ambient [O_3]. On average, the summertime O_3 plant uptake is $117\,\mu\mathrm{mol\,m^{-2}\,day^{-1}}$, with $207\,\mu\mathrm{mol\,m^{-2}\,day^{-1}}$ in the eastern US and $59\,\mu\mathrm{mol\,m^{-2}\,day^{-1}}$ in the western US Following the O_3 stomatal flux, the largest mean GPP reductions are predicted for the eastern US growing season, in the range 4–8 % depending on the O_3 sensitivity applied in the simulations (Fig. 8). Locally, reduction fraction reaches as high as 11–17 % in areas with high [O_3] pollution, such as Michigan, Indiana, Ohio, and states along the northeast coast. Despite high surface [O_3] over mountainous elevated areas in the west (Fig. 4), impacts on GPP are limited due to the low stomatal conductance and low photosynthetic rate there. The Pacific northwestern forests are an exception, with a moderate GPP reduction of 1–7 %. On average, the total summer GPP is reduced by 2–5 % due to O_3 damage effects in the

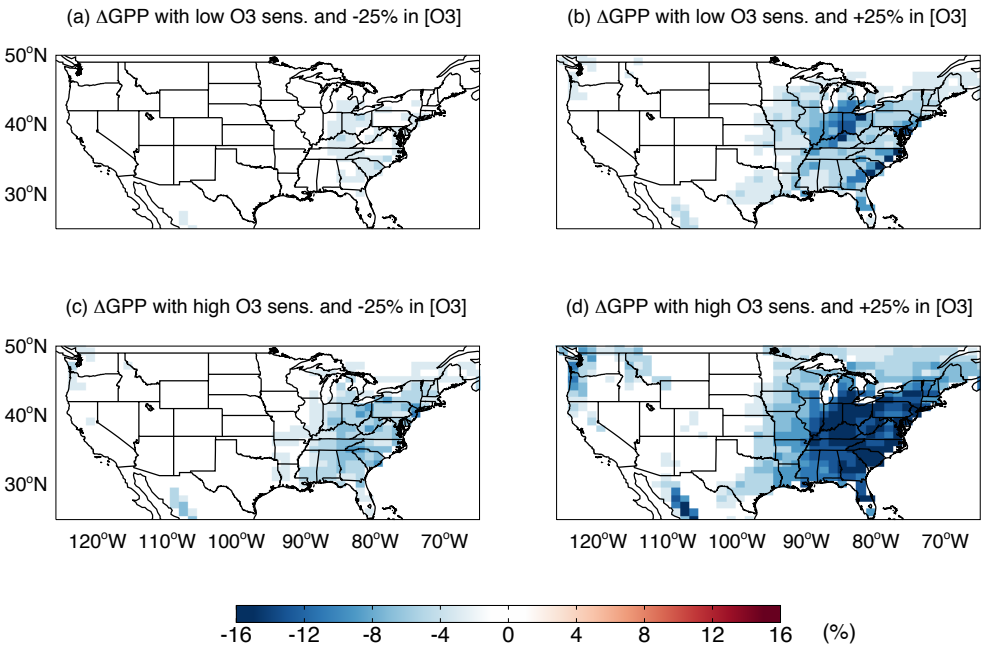

Figure 9. Simulated changes in summer GPP due to **(a, c)** 25 % reduction or **(b, d)** 25 % increase in [O_3] for **(a, b)** low or **(c, d)** high O_3 sensitivity.

US Similar reduction fractions are predicted for the annual GPP.

US surface [O_3] exhibits a decreasing trend over the past 2 decades, especially in the eastern US, due to precursor emission controls (Lefohn et al., 2010). However, the community continues to debate how surface [O_3] will respond to future emissions and climate change. On the one hand, surface [O_3] may decline by the mid 21st century due to large reductions in regional anthropogenic precursor emissions (Wu et al., 2008). On the other hand, climate change effects alone may increase local surface [O_3] due to the warmer, drier, and more stable environment (Leibensperger et al., 2008; Wu et al., 2008). Due to the uncertainty in future surface [O_3] projections, our strategy here is to perform four additional sensitivity experiments with ±25 % changes in [O_3] for each O_3 sensitivity case. Increases of 25 % in [O_3] may reduce GPP in the eastern US by 6–11 %, with a maximum local reduction of 25 % for the high O_3 sensitivity case (Fig. 9d). The damage magnitude with low O_3 sensitivity (Fig. 9b) mimics the present-day estimate with high O_3 sensitivity (Fig. 8b). In contrast, the O_3 damage to the eastern US GPP is as low as 2–4 % in response to 25 % decreases in [O_3] (Fig. 9a, c), suggesting a substantial co-benefit to ecosystem-health of O_3 precursor emissions control.

4 Conclusions

We have performed an updated assessment of O_3 vegetation damage effects on GPP in the US for the 1998–2007 period using the YIBs vegetation model. The semi-mechanistic parameterization of O_3 inhibition on photosynthesis proposed by Sitch et al. (2007) has been implemented into this process-based vegetation model. The simulated O_3 damage effects are consistent with laboratory and field measurements reported in previously published studies. We evaluated the simulated O_3-free and O_3-damaged GPP with in situ measurements from 40 NACP sites. The O_3-free and O_3-damaged GPP simulations capture the seasonality and interannual variability of GPP at most sites. The model GPP biases are lowest at forest and cropland sites but highest at grassland sites. Model GPP is highly sensitive to choice of LAI forcing. Simulations that apply MERRA LAI generally perform better (show lower biases) than those with MODIS LAI. In response to the simulated ambient [O_3] of 30–50 ppbv, simulated GPP decreases by 1–14 % at the NACP sites, depending on the O_3 sensitivity and PFT type. Maximum reductions of 5–14 % occur in two forest sites, where both O_3-free GPP and ambient [O_3] are relatively high. Inclusion of the O_3 damage offers only a small improvement to the simulated annual average GPP at NACP sites (from 3.8 g C m^{-2} day^{-1} to 3.6 g C m^{-2} day^{-1}) such that the model still overestimates the observational average of 3.0 g C m^{-2} day^{-1}. The model GPP overestimate is most likely related to the use of generic PFT-specific photosynthesis parameters and the satellite prescribed LAI that may not represent the local site LAI. In this work, we assumed a coupled response between photosynthesis and stomatal conductance. Emerging research has found that the O_3 vegetation damage effects can actually result in a loss of plant stomatal control, and a consequent

decoupling of the stomatal response from photosynthesis inhibition (Lombardozzi et al., 2012a, b). Treatment of this decoupled response in the YIBs model would lead to a higher level of O_3 flux entering leaves, thus causing stronger damage. Interestingly, this mechanism would provide a way to improve the simulated GPP overestimates. However, other studies have suggested that the O_3 damage to GPP may be offset by the benefits of co-located nitrogen deposition (Ollinger et al., 2002; Felzer et al., 2007), or even limited by carbon-nitrogen interactions (Kvalevag and Myhre, 2013).

Regional simulations for the US yield a summertime GPP (with high sensitivity O_3 damage) of 6.1 g C m^{-2} day^{-1} (9.5 g C m^{-2} day^{-1} in the eastern US and 3.9 g C m^{-2} day^{-1} in the western US). The total carbon uptake was estimated to be 4.43 ± 0.18 Pg C for the summer, accounting for 57–60 % of the annual value of 7.59 ± 0.25 Pg C over the 1998–2007 period. Carbon assimilation rate is suppressed by 4–8 % on average in the summertime eastern US with maximum local damage of 11–17 % in states close to the Great Lakes and along the eastern coast. When [O_3] is decreased by 25 %, O_3 damage to GPP is only 2–4 % in the eastern US, indicating substantial improvements to vegetation health and carbon assimilation rate. Previously, Felzer et al. (2004) found annual average O_3-induced NPP reductions of 3–7 % over the US for 1989–1993 and simulated the largest reductions in states close to the Great Lakes and along the East Coast, where the high O_3 sensitivity of crops makes the dominant contribution. Our study examined O_3 damage effects a decade later than Felzer et al. (2004) but gives consistent results. Qualitatively, this consistency between decades may be explained by the offsetting influences of (i) surface O_3 reductions due to air quality control legislation and (ii) GPP increases due to CO_2-fertilization and rising temperatures. Felzer et al. (2004) estimated a maximum local NPP reduction of 34 %, which is double the maximum of 17 % in our analyses. Furthermore, Felzer et al. (2004) found widespread reductions of > 6 % in the Midwest where there is almost no O_3 impact in this study (Fig. 8). Differences between the studies are mostly likely driven by the use of different vegetation cover and LAI data sets, and the use of a semi-mechanistic flux-based uptake in this study vs. the concentration-based uptake method elsewhere.

The current work has used an off-line approach. Yet, the O_3-vegetation-meteorology system is strongly coupled. For instance, plant productivity itself controls the emission of isoprene, a major O_3 precursor. The O_3-induced modification to stomatal conductance may inhibit evapotranspiration, leading to changes in canopy temperature, precipitation, soil moisture, and other surface hydrology and meteorology (Bernacchi et al., 2007; VanLoocke et al., 2012). In future work, we will study O_3 vegetation damage effects using YIBs embedded within a fully coupled global chemistry–climate model framework in order to account for these feedbacks including altered canopy energy fluxes and partitioning between latent and sensible heat that drive regional climate and hydrology. In addition, the O_3 damage algorithm parameters were calibrated using limited measurements for a few plant species, and were based on biomass yield not photosynthetic rate (Sitch et al., 2007). Future work will exploit recent extensive meta-data analyses (Lombardozzi et al., 2013; Wittig et al., 2007) to refine the ozone damage parameterization in YIBs including the decoupled modification of photosynthesis and stomatal conductance.

Appendix A

Table A1. Descriptions of NACP sites in Canada (CA-) and US (US-)[a].

Site	PFT[b]	Description	Longitude	Latitude	Period
CA-Ca1	ENF	Campbell River	125.3° W	49.9° N	1998–2006
CA-Ca2	ENF	Campbell River	125.3° W	49.9° N	2001–2006
CA-Ca3	ENF	Campbell River	124.9° W	49.5° N	2002–2006
CA-Gro	MF	Groundhog River	82.2° W	48.2° N	2004–2006
CA-Let	GRA	Lethbridge Grassland	112.9° W	49.7° N	2001–2007
CA-Mer	WET	Eastern Peatland	75.5° W	45.4° N	1999–2006
CA-NS1	ENF	UCI Chronosequence	124.9° W	49.5° N	2001–2005
CA-Oas	DBF	BERMS	106.2° W	53.6° N	1997–2006
CA-Obs	ENF	BERMS	105.1° W	54.0° N	2000–2006
CA-Ojp	ENF	BERMS	104.7° W	53.9° N	2000–2006
CA-Qfo	ENF	Quebec	74.3° W	49.7° N	2004–2006
CA-SJ1	ENF	BERMS	104.7° W	53.9° N	2002–2005
CA-SJ2	ENF	BERMS	104.6° W	53.9° N	2004–2006
CA-SJ3	ENF	BERMS	104.6° W	53.9° N	2005–2006
CA-TP4	ENF	Turkey Point	80.4° W	42.7° N	2003–2007
CA-WP1	WET	Western Peatland	112.5° W	55.0° N	2004–2007
US-ARM	GRA[c]	Southern Great Plains	97.5° W	36.6° N	2003–2007
US-Dk3	ENF	Duke Forest	79.1° W	36.0° N	1998–2005
US-Ha1	DBF	Harvard Forest	72.2° W	42.5° N	1992–2006
US-Ho1	ENF	Howland Forest	68.7° W	45.2° N	1996–2004
US-IB1	CRO	Fermi Lab	88.2° W	41.9° N	2006
US-IB2	GRA	Fermi	88.2° W	41.8° N	2005–2006
US-Los	WET	Lost Creek	90.0° W	46.1° N	2001–2006
US-MMS	DBF	Morgan Monroe State Forest	86.4° W	39.3° N	1999–2006
US-MOz	DBF	Missouri Ozark	92.2° W	38.7° N	2005–2007
US-Me2	ENF	Metolius	121.6° W	44.5° N	2002–2007
US-Me3	ENF	Metolius	121.6° W	44.3° N	2004–2005
US-Me5	ENF	Metolius	121.6° W	44.4° N	2000–2002
US-NR1	ENF	Niwot Ridge	105.5° W	40.0° N	1999–2007
US-Ne1	CRO	Mead	96.5° W	41.2° N	2002–2005
US-Ne2	CRO	Mead	96.5° W	41.2° N	2003–2005
US-Ne3	CRO	Mead	96.4° W	41.2° N	2002–2005
US-Pfa	MF	Park Falls	90.3° W	45.9° N	1997–2004
US-SO2	CSH	Sky Oaks	116.6° W	33.4° N	1999–2006
US-Shd	GRA	Shidler	96.7° W	36.9° N	1998–1999
US-Syv	MF	Sylvania Wilderness Area	89.3° W	46.2° N	2002–2006
US-Ton	WSA	Tonzi Ranch	121.0° W	38.4° N	2002–2007
US-UMB	DBF	UMBS	84.7° W	45.6° N	1999–2006
US-Var	GRA	Varia Ranch	121.0° W	38.4° N	2001–2007
US-WCr	DBF	Willow Creek	90.1° W	45.8° N	1999–2006

[a] Site information is adopted from Schaefer et al. (2012), except that the operational time span listed here is only for the period when measurements of GPP are available.
[b] PFT names are as follows: evergreen needleleaf forest (ENF), deciduous broadleaf forest (DBF), grasslands (GRA), croplands (CRO), closed shrublands (CSH), mixed forests (MF), permanent wetlands (WET), and woody savannas (WSA).
[c] The land type at US-ARM is cropland in Schaefer et al. (2012). However, the site is covered by cattle pasture and wheat fields (https://www.arm.gov/sites/sgp), which are more like C3 grassland.

The Supplement related to this article is available online at doi:10.5194/acp-14-9137-2014-supplement.

Acknowledgements. The authors are grateful to B. Felzer and an anonymous reviewer for assistance in evaluating this paper. Data for this analysis was provided by the North American Carbon Program Site Synthesis. Funding for this research was provided by Yale University. This project was supported in part by the facilities and staff of the Yale University Faculty of Arts and Sciences High Performance Computing Center.

Edited by: S. Kloster

References

Ainsworth, E. A.: Rice production in a changing climate: a meta-analysis of responses to elevated carbon dioxide and elevated ozone concentration, Glob. Change Biol., 14, 1642–1650, doi:10.1111/J.1365-2486.2008.01594.X, 2008.

Ainsworth, E. A., Yendrek, C. R., Sitch, S., Collins, W. J., and Emberson, L. D.: The Effects of Tropospheric Ozone on Net Primary Productivity and Implications for Climate Change, Annu. Rev. Plant Biol., 63, 637–661, doi:10.1146/Annurev-Arplant-042110-103829, 2012.

Barr, A., Ricciuto, D., Schaefer, K., Richardson, A., Agarwal, D., Thornton, P., Davis, K., Jackson, B., Cook, R., Hollinger, D., Ingen, C. v., Amiro, B., Andrews, A., Arain, M., Baldocchi, D., Black, T., Bolstad, P., Curtis, P., Desai, A., Dragoni, D., Flanagan, L., Gu, L., Katul, G., Law, B., Lafleur, P., Margolis, H., Matamala, R., Meyers, T., McCaughey, H., Monson, R., Munger, J., Oechel, W., Oren, R., Roulet, N., Torn, M., and Verma, S.: NACP Site: Tower Meteorology, Flux Observations with Uncertainty, and Ancillary Data, Oak Ridge National Laboratory Distributed Active Archive Center, Oak Ridge, Tennessee, USA, 2013.

Bell, N., Koch, D., and Shindell, D. T.: Impacts of chemistry-aerosol coupling on tropospheric ozone and sulfate simulations in a general circulation model, J. Geophys. Res., 110, D14305, doi:10.1029/2004jd005538, 2005.

Bernacchi, C. J., Kimball, B. A., Quarles, D. R., Long, S. P., and Ort, D. R.: Decreases in stomatal conductance of soybean under open-air elevation of [CO_2] are closely coupled with decreases in ecosystem evapotranspiration, Plant Physiol., 143, 134–144, doi:10.1104/Pp.106.089557, 2007.

Bloomer, B. J., Vinnikov, K. Y., and Dickerson, R. R.: Changes in seasonal and diurnal cycles of ozone and temperature in the eastern US, Atmos. Environ., 44, 2543–2551, doi:10.1016/J.Atmosenv.2010.04.031, 2010.

Bonan, G. B., Lawrence, P. J., Oleson, K. W., Levis, S., Jung, M., Reichstein, M., Lawrence, D. M., and Swenson, S. C.: Improving canopy processes in the Community Land Model version 4 (CLM4) using global flux fields empirically inferred from FLUXNET data, J. Geophys. Res., 116, G02014, doi:10.1029/2010jg001593, 2011.

Chen, M., Zhuang, Q., Cook, D. R., Coulter, R., Pekour, M., Scott, R. L., Munger, J. W., and Bible, K.: Quantification of terrestrial ecosystem carbon dynamics in the conterminous United States combining a process-based biogeochemical model and MODIS and AmeriFlux data, Biogeosciences, 8, 2665–2688, doi:10.5194/bg-8-2665-2011, 2011.

Chiariello, N. R.: Phenology of California grasslands, in: Grassland structure and function: California annual grassland, edited by: Huenneke, L. F. and Mooney, H. A., Kluwer Academic Publishers, Dordrecht, 47–58, 1989.

Collatz, G. J., Ball, J. T., Grivet, C., and Berry, J. A.: Physiological and Environmental-Regulation of Stomatal Conductance, Photosynthesis and Transpiration – a Model That Includes a Laminar Boundary-Layer, Agr. Forest Meteorol., 54, 107–136, doi:10.1016/0168-1923(91)90002-8, 1991.

Cooper, O. R., Parrish, D. D., Stohl, A., Trainer, M., Nedelec, P., Thouret, V., Cammas, J. P., Oltmans, S. J., Johnson, B. J., Tarasick, D., Leblanc, T., McDermid, I. S., Jaffe, D., Gao, R., Stith, J., Ryerson, T., Aikin, K., Campos, T., Weinheimer, A., and Avery, M. A.: Increasing springtime ozone mixing ratios in the free troposphere over western North America, Nature, 463, 344–348, doi:10.1038/Nature08708, 2010.

Desai, A. R., Noormets, A., Bolstad, P. V., Chen, J. Q., Cook, B. D., Davis, K. J., Euskirchen, E. S., Gough, C. M., Martin, J. G., Ricciuto, D. M., Schmid, H. P., Tang, J. W., and Wang, W. G.: Influence of vegetation and seasonal forcing on carbon dioxide fluxes across the Upper Midwest, USA: Implications for regional scaling, Agr. Forest Meteorol., 148, 288–308, doi:10.1016/J.Agrformet.2007.08.001, 2008.

Farquhar, G. D., Caemmerer, S. V., and Berry, J. A.: A Biochemical-Model of Photosynthetic Co2 Assimilation in Leaves of C-3 Species, Planta, 149, 78–90, doi:10.1007/Bf00386231, 1980.

Felzer, B., Kicklighter, D., Melillo, J., Wang, C., Zhuang, Q., and Prinn, R.: Effects of ozone on net primary production and carbon sequestration in the conterminous United States using a biogeochemistry model, Tellus B, 56, 230–248, doi:10.1111/J.1600-0889.2004.00097.X, 2004.

Felzer, B., Reilly, J., Melillo, J., Kicklighter, D., Sarofim, M., Wang, C., Prinn, R., and Zhuang, Q.: Future effects of ozone on carbon sequestration and climate change policy using a global biogeochemical model, Clim. Change, 73, 345–373, doi:10.1007/S10584-005-6776-4, 2005.

Felzer, B. S., Cronin, T., Reilly, J. M., Melilloa, J. M., and Wang, X. D.: Impacts of ozone on trees and crops, Comptes rendus Geoscience, 339, 784–798, doi:10.1016/J.Crte.2007.08.008, 2007.

Feng, Z. Z., Kobayashi, K., and Ainsworth, E. A.: Impact of elevated ozone concentration on growth, physiology, and yield of wheat (Triticum aestivum L.): a meta-analysis, Glob. Change Biol., 14, 2696–2708, doi:10.1111/J.1365-2486.2008.01673.X, 2008.

Foot, J. P., Caporn, S. J. M., Lee, J. A., and Ashenden, T. W.: The effect of long-term ozone fumigation on the growth, physiology and frost sensitivity of Calluna vulgaris, New Phytol., 133, 503–511, doi:10.1111/J.1469-8137.1996.Tb01918.X, 1996.

Friend, A. D. and Kiang, N. Y.: Land surface model development for the GISS GCM: Effects of improved canopy physiology on simulated climate, J. Climate, 18, 2883–2902, doi:10.1175/Jcli3425.1, 2005.

Goodale, C. L., Apps, M. J., Birdsey, R. A., Field, C. B., Heath, L. S., Houghton, R. A., Jenkins, J. C., Kohlmaier, G. H., Kurz, W., Liu, S. R., Nabuurs, G. J., Nilsson, S., and Shvidenko, A. Z.: Forest carbon sinks in the Northern Hemisphere, Ecol. Appl., 12, 891–899, doi:10.2307/3060997, 2002.

Grantz, D. A., Vu, H. B., Tew, T. L., and Veremis, J. C.: Sensitivity of Gas Exchange Parameters to Ozone in Diverse C-4 Sugarcane Hybrids, Crop Sci., 52, 1270–1280, doi:10.2135/Cropsci2011.08.0413, 2012.

Gregg, J. W., Jones, C. G., and Dawson, T. E.: Urbanization effects on tree growth in the vicinity of New York City, Nature, 424, 183–187, doi:10.1038/Nature01728, 2003.

Hall, F. G., de Colstoun, E. B., Collatz, G. J., Landis, D., Dirmeyer, P., Betts, A., Huffman, G. J., Bounoua, L., and Meeson, B.: ISLSCP Initiative II global data sets: Surface boundary conditions and atmospheric forcings for land-atmosphere studies, J. Geophys. Res., 111, D22s01, doi:10.1029/2006jd007366, 2006.

Heagle, A. S., Kress, L. W., Temple, P. J., Kohut, R. J., Miller, J. E., and Heggestad, H. E.: Factors influencing ozone dose-yield response relationships in open-top chamber studies, in: Assessment of crop loss from air pollutants, edited by: Heck, W. W., Taylor, O. C., and Tingey, D. T., Elsevier Applied Science, New York, 141–179, 1989.

Henebry, G. M.: Grasslands of the North American Great Plains, in: Phenology: an integrative environmental science, edited by: Schwartz, M. D., Kluwer Academic Publishers, Dordrecht, 157–174, 2003.

Hollaway, M. J., Arnold, S. R., Challinor, A. J., and Emberson, L. D.: Intercontinental trans-boundary contributions to ozone-induced crop yield losses in the Northern Hemisphere, Biogeosciences, 9, 271–292, doi:10.5194/bg-9-271-2012, 2012.

Huntingford, C., Cox, P. M., Mercado, L. M., Sitch, S., Bellouin, N., Boucher, O., and Gedney, N.: Highly contrasting effects of different climate forcing agents on terrestrial ecosystem services, Philos. T. R. Soc. A, 369, 2026–2037, doi:10.1098/Rsta.2010.0314, 2011.

Huntzinger, D. N., Post, W. M., Wei, Y., Michalak, A. M., West, T. O., Jacobson, A. R., Baker, I. T., Chen, J. M., Davis, K. J., Hayes, D. J., Hoffman, F. M., Jain, A. K., Liu, S., McGuire, A. D., Neilson, R. P., Potter, C., Poulter, B., Price, D., Raczka, B. M., Tian, H. Q., Thornton, P., Tomelleri, E., Viovy, N., Xiao, J., Yuan, W., Zeng, N., Zhao, M., and Cook, R.: North American Carbon Program (NACP) regional interim synthesis: Terrestrial biospheric model intercomparison, Ecol. Model., 232, 144–157, doi:10.1016/J.Ecolmodel.2012.02.004, 2012.

Ishii, S., Marshall, F. M., and Bell, J. N. B.: Physiological and morphological responses of locally grown Malaysian rice cultivars (*Oryza sativa* L.) to different ozone concentrations, Water Air Soil Poll., 155, 205–221, doi:10.1023/B:Wate.0000026528.86641.5b, 2004.

Jaffe, D. and Ray, J.: Increase in surface ozone at rural sites in the western US, Atmos. Environ., 41, 5452–5463, doi:10.1016/j.atmosenv.2007.02.034, 2007.

Karnosky, D. F., Skelly, J. M., Percy, K. E., and Chappelka, A. H.: Perspectives regarding 50 years of research on effects of tropospheric ozone air pollution on US forests, Environ. Pollut., 147, 489–506, doi:10.1016/J.Envpol.2006.08.043, 2007.

Kvalevag, M. M. and Myhre, G.: The effect of carbon-nitrogen coupling on the reduced land carbon sink caused by tropospheric ozone, Geophys Res. Lett., 40, 3227–3231, doi:10.1002/Grl.50572, 2013.

King, A. W., Hayes, D. J., Huntzinger, D. N., West, T. O., and Post, W. M.: North American carbon dioxide sources and sinks: magnitude, attribution, and uncertainty, Front. Ecol. Environ., 10, 512–519, doi:10.1890/120066, 2012.

Knyazikhin, Y., Martonchik, J. V., Myneni, R. B., Diner, D. J., and Running, S. W.: Synergistic algorithm for estimating vegetation canopy leaf area index and fraction of absorbed photosynthetically active radiation from MODIS and MISR data, J. Geophys. Res., 103, 32257–32275, doi:10.1029/98jd02462, 1998.

Lefohn, A. S., Shadwick, D., and Oltmans, S. J.: Characterizing changes in surface ozone levels in metropolitan and rural areas in the United States for 1980–2008 and 1994–2008, Atmos. Environ., 44, 5199–5210, doi:10.1016/J.Atmosenv.2010.08.049, 2010.

Leibensperger, E. M., Mickley, L. J., and Jacob, D. J.: Sensitivity of US air quality to mid-latitude cyclone frequency and implications of 1980–2006 climate change, Atmos. Chem. Phys., 8, 7075–7086, doi:10.5194/acp-8-7075-2008, 2008.

Lombardozzi, D., Levis, S., Bonan, G., and Sparks, J. P.: Predicting photosynthesis and transpiration responses to ozone: decoupling modeled photosynthesis and stomatal conductance, Biogeosciences, 9, 3113–3130, doi:10.5194/bg-9-3113-2012, 2012a.

Lombardozzi, D., Sparks, J. P., Bonan, G., and Levis, S.: Ozone exposure causes a decoupling of conductance and photosynthesis: implications for the Ball-Berry stomatal conductance model, Oecologia, 169, 651–659, doi:10.1007/S00442-011-2242-3, 2012b.

Lombardozzi, D., Sparks, J. P., and Bonan, G.: Integrating O_3 influences on terrestrial processes: photosynthetic and stomatal response data available for regional and global modeling, Biogeosciences, 10, 6815–6831, doi:10.5194/bg-10-6815-2013, 2013.

Mulchi, C. L., Slaughter, L., Saleem, M., Lee, E. H., Pausch, R., and Rowland, R.: Growth and Physiological-Characteristics of Soybean in Open-Top Chambers in Response to Ozone and Increased Atmospheric CO_2, Agr. Ecosyst. Environ., 38, 107–118, doi:10.1016/0167-8809(92)90172-8, 1992.

Oleson, K. W., Lawrence, D. M., Bonan, G. B., Flanne, M. G., Kluzek, E., Lawrence, P. J., Levis, S., Swenson, S. C., and Thornton, P. E.: Technical Description of version 4.0 of the Community Land Model (CLM), National Center for Atmospheric Research, Boulder, CONCAR/TN-478+STR, 2010.

Ollinger, S. V., Aber, J. D., Reich, P. B., and Freuder, R. J.: Interactive effects of nitrogen deposition, tropospheric ozone, elevated CO_2 and land use history on the carbon dynamics of northern hardwood forests, Glob. Change Biol., 8, 545–562, doi:10.1046/J.1365-2486.2002.00482.X, 2002.

Pacala, S. W., Hurtt, G. C., Baker, D., Peylin, P., Houghton, R. A., Birdsey, R. A., Heath, L., Sundquist, E. T., Stallard, R. F., Ciais, P., Moorcroft, P., Caspersen, J. P., Shevliakova, E., Moore, B., Kohlmaier, G., Holland, E., Gloor, M., Harmon, M. E., Fan, S. M., Sarmiento, J. L., Goodale, C. L., Schimel, D., and Field, C. B.: Consistent land- and atmosphere-based US carbon sink estimates, Science, 292, 2316–2320, doi:10.1126/Science.1057320, 2001.

Pan, Y. D., Birdsey, R. A., Fang, J. Y., Houghton, R., Kauppi, P. E., Kurz, W. A., Phillips, O. L., Shvidenko, A., Lewis, S. L., Canadell, J. G., Ciais, P., Jackson, R. B., Pacala, S. W., McGuire, A. D., Piao, S. L., Rautiainen, A., Sitch, S., and Hayes, D.: A Large and Persistent Carbon Sink in the World's Forests, Science, 333, 988–993, doi:10.1126/Science.1201609, 2011.

Puma, M. J., Koster, R. D., and Cook, B. I.: Phenological versus meteorological controls on land-atmosphere

water and carbon fluxes, J. Geophys. Res., 118, 14–29, doi:10.1029/2012jg002088, 2013.

Reichle, R. H., Koster, R. D., De Lannoy, G. J. M., Forman, B. A., Liu, Q., Mahanama, S. P. P., and Toure, A.: Assessment and Enhancement of MERRA Land Surface Hydrology Estimates, J Climate, 24, 6322–6338, doi:10.1175/Jcli-D-10-05033.1, 2011.

Ricciuto, D., Schaefer, K., Thornton, P., Davis, K., Cook, R., Liu, S., Anderson, R., Arain, M., Baker, I., Chen, J., Dietze, M., Grant, R., Izaurralde, C., Jain, A., King, A., Kucharik, C., Liu, S., Lokupitiya, E., Luo, Y., Peng, C., Poulter, B., Price, D., Riley, W., Sahoo, A., Tian, H., Tonitto, C., and Verbeeck, H.: NACP Site: Terrestrial Biosphere Model and Aggregated Flux Data in Standard Format, Oak Ridge National Laboratory Distributed Active Archive Center, Oak Ridge, Tennessee, USA, 2013.

Rienecker, M. M., Suarez, M. J., Gelaro, R., Todling, R., Bacmeister, J., Liu, E., Bosilovich, M. G., Schubert, S. D., Takacs, L., Kim, G. K., Bloom, S., Chen, J. Y., Collins, D., Conaty, A., Da Silva, A., Gu, W., Joiner, J., Koster, R. D., Lucchesi, R., Molod, A., Owens, T., Pawson, S., Pegion, P., Redder, C. R., Reichle, R., Robertson, F. R., Ruddick, A. G., Sienkiewicz, M., and Woollen, J.: MERRA: NASA's Modern-Era Retrospective Analysis for Research and Applications, J Climate, 24, 3624–3648, doi:10.1175/Jcli-D-11-00015.1, 2011.

Rigby, M., Prinn, R. G., Fraser, P. J., Simmonds, P. G., Langenfelds, R. L., Huang, J., Cunnold, D. M., Steele, L. P., Krummel, P. B., Weiss, R. F., O'Doherty, S., Salameh, P. K., Wang, H. J., Harth, C. M., Muhle, J., and Porter, L. W.: Renewed growth of atmospheric methane, Geophys. Res. Lett., 35, L22805, doi:10.1029/2008gl036037, 2008.

Rudorff, B. F. T., Mulchi, C. L., Lee, E. H., Rowland, R., and Pausch, R.: Effects of enhanced O-3 and CO_2 enrichment on plant characteristics in wheat and corn, Environ. Pollut., 94, 53–60, doi:10.1016/S0269-7491(96)00050-4, 1996.

Schaefer, K., Schwalm, C. R., Williams, C., Arain, M. A., Barr, A., Chen, J. M., Davis, K. J., Dimitrov, D., Hilton, T. W., Hollinger, D. Y., Humphreys, E., Poulter, B., Raczka, B. M., Richardson, A. D., Sahoo, A., Thornton, P., Vargas, R., Verbeeck, H., Anderson, R., Baker, I., Black, T. A., Bolstad, P., Chen, J. Q., Curtis, P. S., Desai, A. R., Dietze, M., Dragoni, D., Gough, C., Grant, R. F., Gu, L. H., Jain, A., Kucharik, C., Law, B., Liu, S. G., Lokipitiya, E., Margolis, H. A., Matamala, R., McCaughey, J. H., Monson, R., Munger, J. W., Oechel, W., Peng, C. H., Price, D. T., Ricciuto, D., Riley, W. J., Roulet, N., Tian, H. Q., Tonitto, C., Torn, M., Weng, E. S., and Zhou, X. L.: A model-data comparison of gross primary productivity: Results from the North American Carbon Program site synthesis, J. Geophys. Res., 117, G03010, doi:10.1029/2012jg001960, 2012.

Shindell, D. T., Faluvegi, G., Unger, N., Aguilar, E., Schmidt, G. A., Koch, D. M., Bauer, S. E., and Miller, R. L.: Simulations of preindustrial, present-day, and 2100 conditions in the NASA GISS composition and climate model G-PUCCINI, Atmos. Chem. Phys., 6, 4427–4459, doi:10.5194/acp-6-4427-2006, 2006.

Shindell, D. T., Pechony, O., Voulgarakis, A., Faluvegi, G., Nazarenko, L., Lamarque, J.-F., Bowman, K., Milly, G., Kovari, B., Ruedy, R., and Schmidt, G. A.: Interactive ozone and methane chemistry in GISS-E2 historical and future climate simulations, Atmos. Chem. Phys., 13, 2653–2689, doi:10.5194/acp-13-2653-2013, 2013.

Sitch, S., Cox, P. M., Collins, W. J., and Huntingford, C.: Indirect radiative forcing of climate change through ozone effects on the land-carbon sink, Nature, 448, 791–794, doi:10.1038/Nature06059, 2007.

Spitters, C. J. T., Toussaint, H. A. J. M., and Goudriaan, J.: Separating the Diffuse and Direct Component of Global Radiation and Its Implications for Modeling Canopy Photosynthesis. 1. Components of Incoming Radiation, Agr. Forest Meteorol., 38, 217–229, doi:10.1016/0168-1923(86)90060-2, 1986.

Taylor, M. D., Sinn, J. P., Davis, D. D., and Pell, E. J.: The impact of ozone on a salt marsh cordgrass (Spartina alterniflora), Environ. Pollut., 120, 701–705, 2002.

Unger, N.: Global climate impact of civil aviation for standard and desulfurized jet fuel, Geophys. Res. Lett., 38, L20803, doi:10.1029/2011gl049289, 2011.

Unger, N. and Pan, J. L.: New Directions: Enduring ozone, Atmos. Environ., 55, 456–458, doi:10.1016/J.Atmosenv.2012.03.036, 2012.

Unger, N., Harper, K., Zheng, Y., Kiang, N. Y., Aleinov, I., Arneth, A., Schurgers, G., Amelynck, C., Goldstein, A., Guenther, A., Heinesch, B., Hewitt, C. N., Karl, T., Laffineur, Q., Langford, B., A. McKinney, K., Misztal, P., Potosnak, M., Rinne, J., Pressley, S., Schoon, N., and Serça, D.: Photosynthesis-dependent isoprene emission from leaf to planet in a global carbon-chemistry-climate model, Atmos. Chem. Phys., 13, 10243–10269, doi:10.5194/acp-13-10243-2013, 2013.

von Caemmerer, S. and Farquhar, G. D.: Some Relationships between the Biochemistry of Photosynthesis and the Gas-Exchange of Leaves, Planta, 153, 376–387, 1981.

VanLoocke, A., Betzelberger, A. M., Ainsworth, E. A., and Bernacchi, C. J.: Rising ozone concentrations decrease soybean evapotranspiration and water use efficiency whilst increasing canopy temperature, New Phytol., 195, 164–171, doi:10.1111/J.1469-8137.2012.04152.X, 2012.

Wittig, V. E., Ainsworth, E. A., and Long, S. P.: To what extent do current and projected increases in surface ozone affect photosynthesis and stomatal conductance of trees? A meta-analytic review of the last 3 decades of experiments, Plant Cell Environ., 30, 1150–1162, doi:10.1111/J.1365-3040.2007.01717.X, 2007.

Wu, S. L., Mickley, L. J., Leibensperger, E. M., Jacob, D. J., Rind, D., and Streets, D. G.: Effects of 2000–2050 global change on ozone air quality in the United States, J. Geophys. Res., 113, D06302, doi:10.1029/2007jd008917, 2008.

Xiao, J. F., Zhuang, Q. L., Law, B. E., Chen, J. Q., Baldocchi, D. D., Cook, D. R., Oren, R., Richardson, A. D., Wharton, S., Ma, S. Y., Martin, T. A., Verma, S. B., Suyker, A. E., Scott, R. L., Monson, R. K., Litvak, M., Hollinger, D. Y., Sun, G., Davis, K. J., Bolstad, P. V., Burns, S. P., Curtis, P. S., Drake, B. G., Falk, M., Fischer, M. L., Foster, D. R., Gu, L. H., Hadley, J. L., Katul, G. G., Roser, Y., McNulty, S., Meyers, T. P., Munger, J. W., Noormets, A., Oechel, W. C., Paw, K. T., Schmid, H. P., Starr, G., Torn, M. S., and Wofsy, S. C.: A continuous measure of gross primary production for the conterminous United States derived from MODIS and AmeriFlux data, Remote Sens. Environ., 114, 576–591, doi:10.1016/J.Rse.2009.10.013, 2010.

Zhang, L., Su, B. Y., Xu, H., and Li, Y. G.: Growth and photosynthetic responses of four landscape shrub species to elevated ozone, Photosynthetica, 50, 67–76, doi:10.1007/S11099-012-0004-Z, 2012.